JOURNAL OF THERMOPHYSICS AND HEAT TRANSFER
Vol. 33, No. 4, October–December 2019

Cooling-Water Leakage Diagnosis Using Optical Emission Spectroscopy for a Large-Scale Arc-Heated Facility

X. Lin*
State Key Laboratory of High-Temperature Gas Dynamics, 100190 Beijing, People's Republic of China
D. B. Ou,† J. L. Peng,‡ and H. Zeng‡
China Academy of Aerospace Aerodynamics, 100074 Beijing, People's Republic of China
and
F. Li§ and X. L. Yu¶
State Key Laboratory of High-Temperature Gas Dynamics, 100190 Beijing, People's Republic of China

DOI: 10.2514/1.T5651

A technique for optical emission spectroscopy is developed and deployed in the detection of cooling-water leakage in an arc-heated wind tunnel at China Academy of Aerospace Aerodynamics. The arc heater operates at temperatures of 5000–9000 K and pressures of 2–6 atm. Two mass-average enthalpy conditions, 18.7 MJ/kg (test 1) and 16.4 MJ/kg (test 2), are studied. From the spectral characteristics of the normal and leakage spectra, the 656.28-nm emission spectral line of atomic hydrogen ($H_{656.28}$) and the 777.19-nm emission spectral line of atomic oxygen ($O_{777.19}$) are selected for coolant-leakage detection in the arc heater. Given the emission intensity ratio of $H_{656.28}$ and $O_{777.19}$, detection limits for the mass flow of the leaking water are derived; for tests 1 and 2, they are 18.5–0.94 g/s and 2.12–0.98 g/s, corresponding to equilibrium temperatures ranging from 6000 to 8000 K and 5500 to 7500 K, respectively. This work demonstrates the feasibility and potential of the optical emission spectroscopy technology in high-enthalpy arc heater health diagnosis, especially in regard to the coolant leakage diagnosis.

Nomenclature

A	=	integrated emission intensity, a.u.
A_{ki}	=	Einstein transition probability, s^{-1}
E	=	energy, cm^{-1}
G	=	air mass flow rate, $g \cdot s^{-1}$
g	=	degeneracy
H_0	=	mass-average enthalpy, $MJ \cdot kg^{-1}$
h	=	Planck constant, $J \cdot s$
k	=	Boltzmann constant, $J \cdot K^{-1}$
M	=	molar mass, $g \cdot mol^{-1}$
$\dot{m}$	=	mass flow rate, $g \cdot s^{-1}$
n	=	number density, cm^{-3}
Q	=	electronic partition function
T	=	equilibrium temperature, K
T_0	=	total temperature, K
v	=	= transition frequency, s^{-1}

Subscripts

H	=	hydrogen atom
i	=	electronic level in the upper state
k	=	electronic level in the lower state
O	=	oxygen atom
0	=	ground state

Received 10 October 2018; revision received 29 January 2019; accepted for publication 21 February 2019; published online Open Access 24 May 2019.

*Senior Engineer, Institute of Mechanics, Chinese Academy of Sciences; also China Academy of Aerospace Aerodynamics, 100074 Beijing, People's Republic of China; linxin_bit@163.com.
†Professor, Beijing Key Laboratory of Arc Plasma Application Equipment.
‡Engineer, Beijing Key Laboratory of Arc Plasma Application Equipment.
§Associate Professor, Institute of Mechanics, Chinese Academy of Sciences; lifei@imech.ac.cn (Corresponding Author).
¶Professor, Institute of Mechanics, Chinese Academy of Sciences; also School of Engineering Science, University of Chinese Academy of Sciences, 100049 Beijing, People's Republic of China; xlyu@imech.ac.cn (Co-Corresponding Author).

I. Introduction

ARC-HEATED facilities provide a crucial ground testing service to aerothermodynamics research in producing high-enthalpy environments similar to those experienced during hypersonic vehicle flights [1–4]. These facilities are generally used for various applications, such as quantifying the performance of a thermal protection system (TPS), characterizing the surface catalytic effect of thermal protection materials, testing scramjet engines, and understanding boundary-layer transitions [5–7]. A high-power electric arc discharge is used to create a high-temperature gas stream during arc-heating operations. The electrodes and arc heater components must be cooled by high-pressure water because of the intensive heat fluxes generated by the arc root at the electrode surface and the high-enthalpy environment in the arc heater [8,9]. An external magnetic field and a vortex gas flow are also commonly used to distribute the thermal load on the electrodes [10–12].

Unfortunately, erosion of these water-cooled electrodes is inevitable, and this may lead to a serious contamination of the test gas, a reduction in service life, and a loss in reliability of the arc-heated facilities [13–16]. Especially for long-duration (hundreds or even thousands of seconds) aerodynamic heating tests, there exists a risk of the coolant leaking from the electrodes due to the accumulation erosion of the electrode materials. When this happens, and the arc heater is not shut down in time, the leaking coolant causes an internal short circuit in the arc heater, which leads to a rapid expansion of the ablation, and even causes the arc heater to be completely damaged. This not only seriously delays the progress of the aerodynamic heating test but also causes huge economic losses. In addition to leak-induced damage, some practical issues such as insufficient machining accuracy of the coolant channel inside the arc heater or blockage of the connecting pipes easily lead to severe local erosion of the electrode and the arc heater components.

The erosion of electrodes remains one of the most important and challenging issues in the high-enthalpy arc-heated facilities.

Experimental investigations of the physics behind the erosion of electrodes have been performed by many researchers [17–23]. Guile et al. [17] explored the influence of the electrode surface temperature on the erosion of cold copper cathodes. The surface temperature was observed to be the most essential factor influencing copper cathode erosion in magnetically driven arcs and was later confirmed by Essiptchouk et al. [18]. Teste et al. [19] studied the influence of the electrode gap on copper electrode erosion. Meanwhile, several numerical models have been established to provide insight into the mechanism of electrode erosion [24–28]. Coulombe and Meunier [24] developed a numerical model to describe the attachment of an electric arc on a vaporizing nonrefractory cathode. Marotta and Sharakhovsky [25–27] proposed a thermophysical model to estimate copper cathode operating regimes in which minimal erosion occurs. Webb and Sheeley [28] developed a modified mass loss model to investigate the effects of shear on arc heater electrodes.

However, all previous experimental and numerical studies focused on investigating the mechanism and key factors on electrode erosion. Although they are useful for understanding the electrode erosion mechanism and a guide to optimal designs of electrodes with minimum erosion, to the best of our knowledge, there has been no effort targeting at the investigation of accurate diagnosis the beginning of micro-leakage in a high-enthalpy arc heater and assessing the mass flows of leaking water quantitatively. Arc heaters are suspect to severe damage due to the late detection of leaks. Therefore, the development of fast response and accurately quantitative diagnostic techniques for leak detection of coolant in a high-enthalpy arc heater would be highly beneficial. Because of the harsh conditions inside the high-enthalpy arc heater, especially in a large-scale facility, choices of diagnostic methods are limited, but nonintrusive spectroscopy-based techniques offer an opportunity. Optical emission spectroscopy (OES) is a powerful tool to probe atoms and molecules, having been used in many areas such as chemical kinetics, nonequilibrium radiation, and plasma diagnostics [29–34].

This paper describes an experimental investigation of the application of OES in the leak detection of cooling water for a large-scale (50 MW) arc-heated wind tunnel (FD-17) at the China Academy of Aerospace Aerodynamics (CAAA). Optical measurements are achieved using a water-cooled optical disk designed with an optical access port and an extension tube. Depending on the spectral characteristics of the high-temperature flow field in the FD-17 arc heater, the 656.28-nm emission spectral line of atomic hydrogen ($H_{656.28}$) and the 777.19-nm emission spectral line of atomic oxygen ($O_{777.19}$) are used for determining and evaluating the early stage of micro-leaking water in the normal operation of the arc heater. Water leakage failure occurring under two test conditions is successfully diagnosed, and the mass flow of leaking water is deduced from the integrated atomic line intensity ratio $I_{H_{656.28}}/I_{O_{777.19}}$ based on the local thermal equilibrium. Finally, a detailed discussion of the sensitivity and potential of the experimental approach is also given.

II. Experimental Apparatus

A. FD-17 Arc-Heated Wind Tunnel

The experimental investigations are carried out in the FD-17 arc-heated wind tunnel at CAAA. The FD-17 is a large-scale constricted arc-heated facility and is capable of generating high-enthalpy hypersonic flow for tens of minutes. The FD-17 consists of a 50-MW arc heater, a convergent-divergent supersonic nozzle, a test chamber, and a vacuum system, as shown in Fig. 1. The arc heater consists of an upstream anode and a downstream cathode, separated by a constrictor tube made by hundreds of water-cooled electrically isolated copper disks. The performance of the arc heater varies by changing the length of the constrictor. To reduce electrode erosion, both anode and cathode assemblies consist of several electrode disks separated by an electrically isolated interelectrode segment, and the total current can be decomposed to each electrode. A current-induced magnetic field is applied to further reduce the electrode erosion by rapidly spinning the arc spot on the electrode surface and improving the heat transfer to gas near the electrodes. Argon gas is injected to sheathe each electrode disk to reduce the breakdown voltage required to start the arc. Test air is tangentially injected into the constrictor tube and heated by the arc column established between the anode and the cathode. The arc-heated plasma accelerates through a convergent-divergent nozzle and flows into the test chamber at supersonic speeds over a TPS test model positioned on the sting arms. Typically, the FD-17 arc heater operates at temperatures of 5000–9000 K and pressures of 2–6 atm. To regulate the flow enthalpy to the desired conditions in a convenient manner, a suitable amount of room-temperature air is tangentially injected from the nozzle inlet (called "cold-air" injection). The operating conditions of the facility are regulated using the applied electric current and total mass flow to produce the required chamber pressure and mass-average enthalpy. The mass-average enthalpy is determined by the sonic throat method [35]; the total temperature is derived from charts of the equilibrium flow properties of air in hypervelocity nozzles [36]. In our studies, two operating conditions were investigated, as shown in Table 1.

B. Optical Measurements

Optical measurements were performed via an optical disk downstream of the cathode and upstream of the nozzle. The optical disk was also designed with a high-pressure water-cooling system to avoid overheated damage of the disk from high-temperature flow erosion. The geometric configuration of the optical disk (Fig. 1, bottom right corner) includes an optical access port to the cross-section centerline. An extension tube, equipped with a 4-mm-diam quartz window and a quartz lens of focal length 5 mm, is threaded into the optical port to provide beam collimation. The emission was then collected through a 20-m-length optical fiber located at the inner end of the extension. The optical fiber was connected to an adjustable attenuator to adjust the radiation signal strength. Emission spectra were recorded using a spectrometer (QE65 Pro, Ocean Optics Inc., Largo, FL) equipped with a charge-coupled device camera

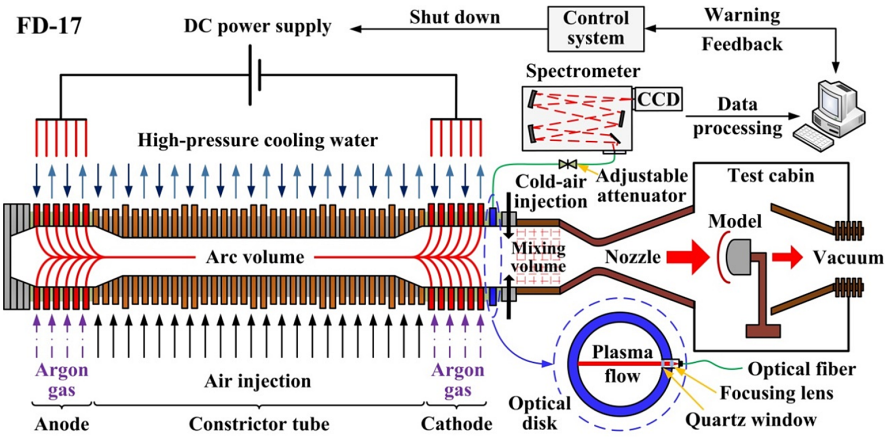

Fig. 1 Schematic of the experimental setup of the FD-17 and emission spectroscopy measurement system.

Table 1 Test conditions

Test condition	Air mass flow rate G, g · s^{-1}	Mass-average enthalpy H_0, MJ · kg^{-1}	Total temperature T_0, K
1	846	18.7	≈7000
2	1030	16.4	≈6500

(Hamamatsu Photonics, Iwata City, Japan) with a 1024 × 58 pixel array. To achieve a fast response with millisecond temporal resolution and a sufficient signal-to-noise ratio (SNR), the exposure time of the camera was set to 20 ms with a repetition rate of 50 Hz. The nominal spectral range of the spectrometer was 300–900 nm, and the entrance slit was fixed at 10 μm. The full-width at half-maximum (FWHM) of the spectral resolution was measured using a He-Ne laser beam and was equal to 1.2 nm with a Voigt profile. The optical system was calibrated in terms of the relative intensity in the target range (600–800 nm) using a National Institute of Standards and Technology traceable quartz–tungsten–halogen standard reference lamp (model 63945, Oriel Instruments, Stratford, CT).

The raw spectral data are analyzed and processed in real time using software independently developed by the laboratory. By accumulating multiple test data in the future and perfecting of the water leakage criteria, the software is linked to the FD-17 control system so that the FD-17 quickly (within 0.1 s) and automatically shuts down when a warning of the water leakage is issued, thereby minimizing arc-heater losses.

III. Spectral Analysis

A. Characteristics of the Emission Spectra at the Beginning of Water Leaking in the Arc Heater

The FD-17 operates at a high-temperature regime (5000–9000 K), where all of the molecular oxygen in the arc-heated air flow is assumed to have dissociated. The spectral intensities of the arc-heated gases before and after a cooling-water leak were measured under two different test conditions for a comparative analysis, as shown in Fig. 2. For each test, the experimental spectra for the arc heater under normal operations (called normal spectra) and when water begins to leak in the arc heater (called leakage spectra) were obtained (Fig. 2, black and red solid lines, respectively). In the wavelength region of 600–800 nm, the radiation mainly consists of the strong atomic lines of oxygen and nitrogen and the continuum radiation. Note that there is an obvious $H_{656.28}$ emission when water begins to leak in the arc heater; however, it does not exist when the arc heater is operating normally. Moreover, the continuum radiation intensity of the leakage spectrum, as well as the intensity of the $O_{777.19}$ emission, matches very well with those of the normal spectrum. On the one hand, this phenomenon indicates that the mass flow of the leaking water is extremely small when water begins to leak in the arc heater and does not affect the normal operation of the arc heater. Meanwhile, there are no measurable variation in pressure, electric current, and voltage parameters at the beginning of leakage. On the other hand, the appearance of the $H_{656.28\,nm}$ emission indicates that micro-leakage water dissociated immediately into hydrogen and oxygen atoms, and the strong emission intensity of the $H_{656.28\,nm}$ emission offers an acceptable SNR under the two high-enthalpy conditions. From the spectral characteristics of the normal and leakage spectra, the $H_{656.28}$ emission was selected for the detection of leaking coolant, whereas the $O_{777.19}$ emission was used to monitor the operating status of the arc heater.

B. Determination Methods for the $O_{777.19}$ and $H_{656.28}$ Emission Intensities

Depending on the characteristics of the normal and leakage spectra, different intensity definitions were used in our studies to analyze the intensities of the $O_{777.19}$ and $H_{656.28}$ emissions quantitatively. For the $O_{777.19}$ emission, its intensity is defined as the integrated emission intensity of the atomic line because it is a signature of the chemical reaction among high-temperature air with very high emission efficiency; its intensity variation visually reflects the operation status of the arc heater in our studies. The data processing procedure includes three step. First, for each measured emission signal as shown in Fig. 3, a polynomial is fitted to the nonradiation wings of the emission feature to extrapolate a zero-emission baseline. Here, the baseline is fitted with a fifth-order polynomial. Second, a plot of the emission feature can be constructed according to the baseline obtained in the first step. According to an accurate calibration of the spectral resolution, a Voigt profile is used to fit the emission feature. Third, the integrated emission intensity can be calculated by taking the integral of the entire emission line shape over the wavelength, as shown by the red shadow in Fig. 3.

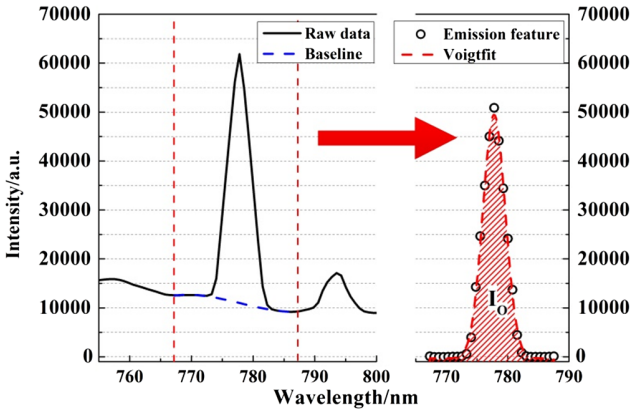

Fig. 3 Raw emission spectrum and data processing for $O_{777.19}$ emission intensity determination in test 1.

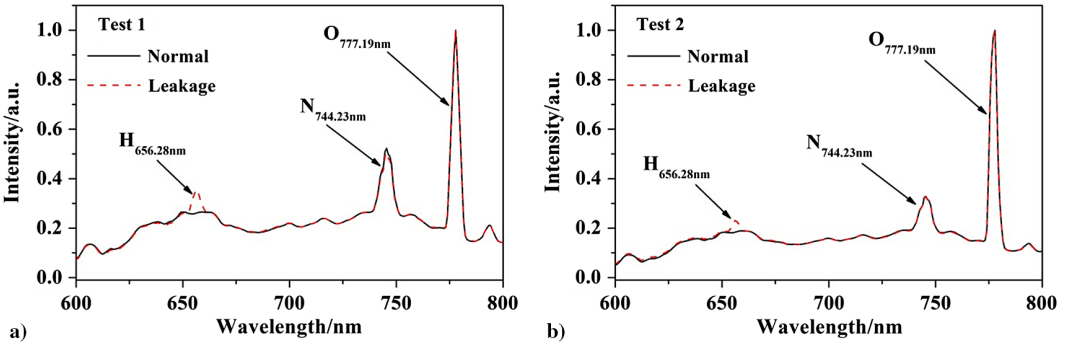

Fig. 2 Spectral characteristics of the arc-heated gases under normal operations and when water begins to leak in arc heater for the two test conditions.

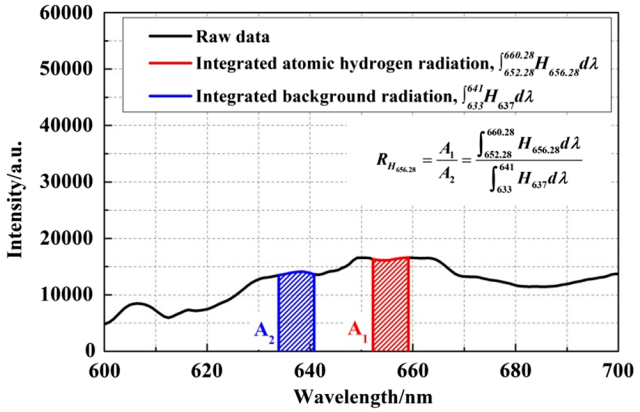

Fig. 4 Raw emission spectrum and data processing for the determination of the $H_{656.28}$ emission intensity ratio for test 1.

However, this processing method is not suitable for the $H_{656.28}$ emission. This is because $H_{656.28}$ exists only when water leakage occurs. The signal intensity is also relatively weak compared with that of the background continuum radiation, making it difficult to identify the profile of the $H_{656.28}$ spectrum accurately, and thereby making the previous method ineffective. In addition, the profile of the background continuum radiation is different for different running conditions of the arc heater and is also affected by fluctuations in current, voltage, and air mass flow rate. Based on the analysis of spectral data of a large number of tests, we propose an "intensity-ratio" method to process the $H_{656.28}$ intensity. As shown in Fig. 4, this intensity ratio is defined as the ratio between the integrated radiation intensity at the central wavelength of 656.28 nm and the integrated background radiation; both have bandwidths of 8 nm. The background radiation is selected as a spectral region near $H_{656.28}$ and not disturbed by the atomic lines. Referring to Fig. 2, wavelength 637 nm is selected as the central wavelength of the background radiation. Because the two integrated radiation intensities are obtained with adjacent central wavelengths and the same integrated bandwidth, the ratio of these two integrals helps to eliminate the interference caused by variations in the continuum radiation and fluctuations of the related operating parameters (air mass flow rates, current, and voltage).

IV. Results and Discussion

A. Determination of the $O_{777.19}$ Emission Intensity and $H_{656.28}$ Emission Intensity Ratio

Figure 5 presents temporal profiles of $O_{777.19}$ emission intensity and $H_{656.28}$ emission intensity ratio using OES for test 1. As shown in Fig. 5, the evolution of $O_{777.19}$ emission intensity intuitively reflects the operating status of the arc heater. The entire test time can be divided into three major stages: startup, steady, and shutdown. The arc startup period (0–10.6 s) comprises the turn-on sequence for the arc heater when the discharge is initiated in argon after about 0.6 s, the addition of a small amount of air after about 1.5 s, and the stepwise increase in mass flow, current, and voltage to tailor the enthalpy to the desired test 1 after about 10.6 s. Once this condition is achieved, all facility input parameters are held constant and the arc heater achieves a steady state (10.6–14 s). From the plot (Fig. 5), the $O_{777.19}$ emission intensity increases stepwise (0–10.6 s) and then remain stable (10.6–14 s).

However, for the $H_{656.28}$ radiation, although the $O_{777.19}$ emission intensity gradually increases, its relative intensity ratio remains basically constant ($R_{H_{656.28}} \approx 1.1$) until about 12.5 s. The experimental results demonstrate that, on the one hand, there are no $H_{656.28}$ emissions during this time range, which means that there is no water leakage in the arc heater. On the other hand, it confirms the previous view that the "intensity-ratio" method for the $H_{656.28}$ emission eliminates effectively the interference caused by variations of the continuum radiation and fluctuations of the related operating parameters. Then, after about 12.5 s, a sudden jump in the $H_{656.28}$ emission intensity ratio indicates that the arc heater begins to leak. However, the fluctuation of the $O_{777.19}$ emission intensity is not obvious during the time range of 12.5–14 s, indicating that the mass flow of the leaking water is very small during this period and the dose does not affect the normal operation of the arc heater significantly. Finally, after about 14 s, the $O_{777.19}$ emission intensity rapidly decreases, as does the $H_{656.28}$ emission intensity ratio when it reaches its maximum value at about 14.4 s. The main reason for this phenomenon may be severe electrode erosion at that moment leading to a rapid increase in the leakage of cooling water, which eventually results in the arc-heated plasma being extinguished.

The same analysis is used for test 2, and the temporal profiles of the $O_{777.19}$ emission intensity and $H_{656.28}$ emission intensity ratio are simultaneously shown in Fig. 6. It is clear in the figure that there are some discrepancies in the $O_{777.19}$ radiation measurements compared with Fig. 5. One relates to the evolution of the $O_{777.19}$ emission intensity during the startup period (2.5–17.5 s), which is quite different from that of test 1. This is because the adjustment mode of the input parameters changes from a stepwise increase to a linear increase under test 2 conditions. Another discrepancy is that because the enthalpy in test 2 is lower than that of test 1, the $O_{777.19}$ emission intensity is weaker than that of test 1 during steady state (17.5–40 s).

Consistent with test 1, the emission intensity ratio for $H_{656.28}$ radiation also stabilizes at around 1.1 from 2.5 to 29.6 s. The experimental results further illustrate the reliability and anti-interference of the "intensity-ratio" method for $H_{656.28}$. From 29.6 s to arc-heater shutdown, the $H_{656.28}$ emission intensity ratio increases, whereas there is no abnormal fluctuation for the $O_{777.19}$ emission intensity. For both the $O_{777.19}$ emission intensity and $H_{656.28}$ emission intensity ratio, the respective time evolutions are similar to those from test 1 when the arc heater is leaking. Note that the peak value and the rise rate of the $H_{656.28}$ emission intensity ratio are significantly lower than that of test 1. We believe that the main reason for the difference is that the amount of the leaking water in test 2 is much less than that of test 1, and this amount indirectly characterizes the extent of damage for the arc heater in both tests.

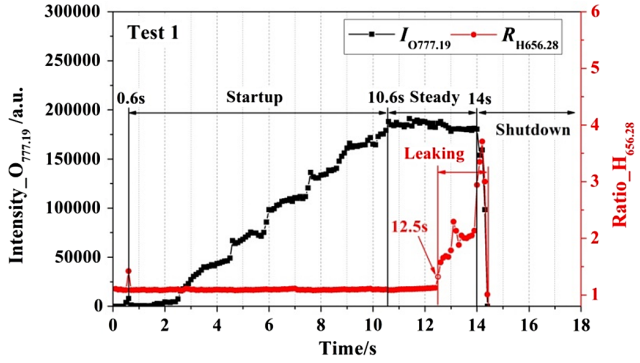

Fig. 5 Evolution of the $O_{777.19}$ emission intensity and the $H_{656.28}$ emission intensity ratio in test 1.

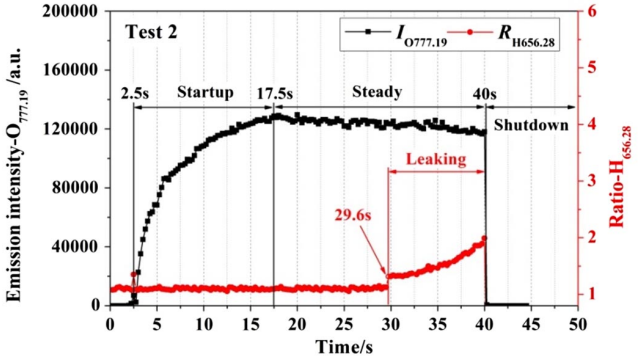

Fig. 6 Evolution of the $O_{777.19}$ emission intensity and the $H_{656.28}$ emission intensity ratio in test 2.

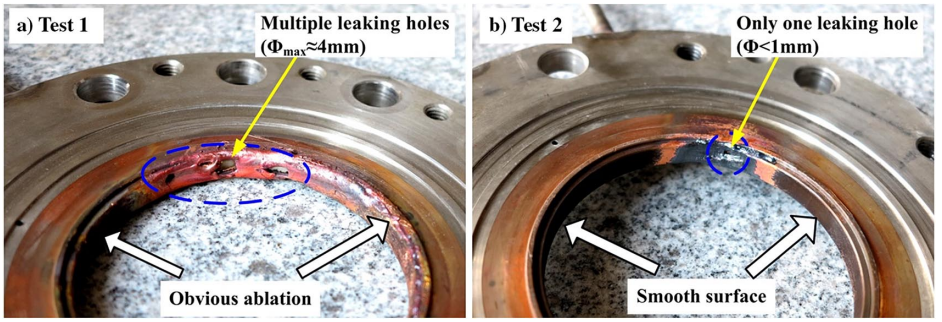

Fig. 7 Damaged electrode disks of the arc heater due to water leakage in the two tests.

To verify this hypothesis, damage to the electrode disks of the arc heater due to water leakage from the two tests were assessed by a photo comparison, as shown in Fig. 7. For test 1, multiple leak holes are visible (Fig. 7a), the largest being approximately 4 mm in diameter; significant ablation is seen in the inner wall of the electrode disk, caused by a short circuit in the arc heater from the presence of a large amount of leaking water. However, for test 2, the ablation and erosion of the damaged electrode disk is much lighter than that of test 1. This is because the amount of leaking water is very small, the water is almost completely vaporized and disassociated, and the water has not caused serious short circuits in the arc heater.

B. Sensitivity Analysis of the Optical Measurement Method

The atomic emission intensity is described as

$$I = h\upsilon_{ki}A_{ki}n_k \tag{1}$$

where I is the emission intensity; h is the Planck constant; υ_{ki} is the transition frequency; A_{ki} is the Einstein transition probability; and n_k is the upper-state number density. In this study, we make equilibrium assumptions with regard to the thermodynamic state of the heated gas in the arc heater. Because of the high pressures in the plenum region of the arc heater, the assumption seems reasonable in that region of the flow. The assumption is also discussed and justified in detail in the work of Winter et al. [37–39]. For gases in local thermodynamic equilibrium, the distribution of the electronic states depends expressly on the equilibrium temperature T. The number density of the upper state n_k in an electronic transition is related to the ground-state number density n_0 through the Boltzmann relation,

$$\frac{n_k}{n_0} = \frac{g_k}{Q(T)}\exp\left(-\frac{E_k}{kT}\right) \tag{2}$$

where g_k is the upper state degeneracy; E_k is the upper state energy; k is the Boltzmann constant; and $Q(T)$ is the electronic partition function. Important spectroscopic parameters relevant to the $H_{656.28}$ and $O_{777.19}$ are listed in Table 2.

The electronic partition functions for atomic hydrogen and oxygen are equal to [40]

$$Q_H(T) = 2 \tag{3}$$

and

$$Q_O(T) = 5 + 3\exp(-228/T) + \exp(-326/T) \tag{4}$$

Substituting Eq. (2) into Eq. (1), the emission intensity is described by

Table 2 Fundamental spectroscopy parameters for the electronic transitions measured in this study

Atom	υ_{ki}, nm	A_{ki}, μs^{-1}	g_i	g_k	E_k, cm^{-1}
H	656.28	53.88	4	6	97,492
O	777.19	36.9	5	15	86,631

$$I = h\upsilon_{ki}A_{ki}n_0\frac{g_k}{Q(T)}\exp\left(-\frac{E_k}{kT}\right) \tag{5}$$

The emission intensity ratio is then

$$\frac{I_H}{I_O} = \frac{n_{0H}}{n_{0O}}\frac{A_{kiH}}{A_{kiO}}\frac{\upsilon_{kiH}}{\upsilon_{kiO}}\frac{g_{kH}}{g_{kO}}\frac{Q_O(T)}{Q_H(T)}\exp\left(\frac{E_{kO}-E_{kH}}{kT}\right) \tag{6}$$

Under the two experimental conditions in our work ($H_0 = 18.7\ MJ\cdot kg^{-1}$, $T \approx 7000$ K; $H_0 = 16.5\ MJ\cdot kg^{-1}$, $T \approx 6500$ K), theoretically all of oxygen molecules in the arc-heated air flow are dissociated into oxygen atom. From our previous spectral analysis and experimental results, micro-leaking water does not affect the normal operation of the arc heater when water begins to leak in arc heater. All the water molecules will be immediately decomposed into hydrogen atom and oxygen atom. The dissociation reactions of O_2 and H_2O are as follows:

$$O_2 \rightarrow 2O \tag{7}$$

$$H_2O \rightarrow 2H + O \tag{8}$$

The number density of H is directly proportional to the mass flow of the leaking water $\dot{m}_{H_2O}$, whereas the number density of O is proportional to the mass flows of air $\dot{m}_{air}$ and of leaking water $\dot{m}_{H_2O}$. As air contains about 21% O_2 and $\dot{m}_{air}$ is known, $\dot{m}_{H_2O}$ can be determined as a function of temperature T and the measured emission intensity ratio I_H/I_O. Consequently, the Eq. (6) becomes

$$\frac{I_H}{I_O} = \frac{2\times(\dot{m}_{H_2O}/M_{H_2O})}{2\times(0.21\times\dot{m}_{air}/M_{O_2}) + (\dot{m}_{H_2O}/M_{H_2O})} \times\frac{A_{kiH}}{A_{kiO}}\frac{\upsilon_{kiH}}{\upsilon_{kiO}}\frac{g_{kH}}{g_{kO}}\frac{Q_O(T)}{Q_H(T)}\exp\left(\frac{E_{kO}-E_{kH}}{kT}\right) \tag{9}$$

Figure 8 presents typical integrated intensity measurements for $H_{656.28}$ and $O_{777.19}$ emission under test 2 condition. The processing method is the same as the intensity determination method for the $O_{777.19}$ emission, as discussed in Sec. IV.A. The bottom panel of Fig. 8a shows the experimental emission line shape fitted with a Voigt profile for $H_{656.28}$, whereas the top portion shows the fitting residual, which is less than 5% of the peak emission throughout the line profile. The corresponding fitting residual yields an overall uncertainty of less than 3% in the integrated emission intensity measurement. The same analysis is used for the $O_{777.19}$ emission, and the results are presented in Fig. 8b. The Voigt profile fit results in an uncertainty of ~2% in in the integrated emission intensity. The overall uncertainty in the intensity ratio between $H_{656.28}$ emission and $O_{777.19}$ emission is therefore about 5%.

To verify that the assumption of micro-leakage holds and to analyze the sensitivity of the optical method, the emission intensity ratios were calculated at 12.5 and 29.6 s (Figs. 5 and 6, respectively) when water leakage begins in Tests 1 and 2. The measured ratios between the $H_{656.28}$ and $O_{777.19}$ emission intensities for tests 1 and 2

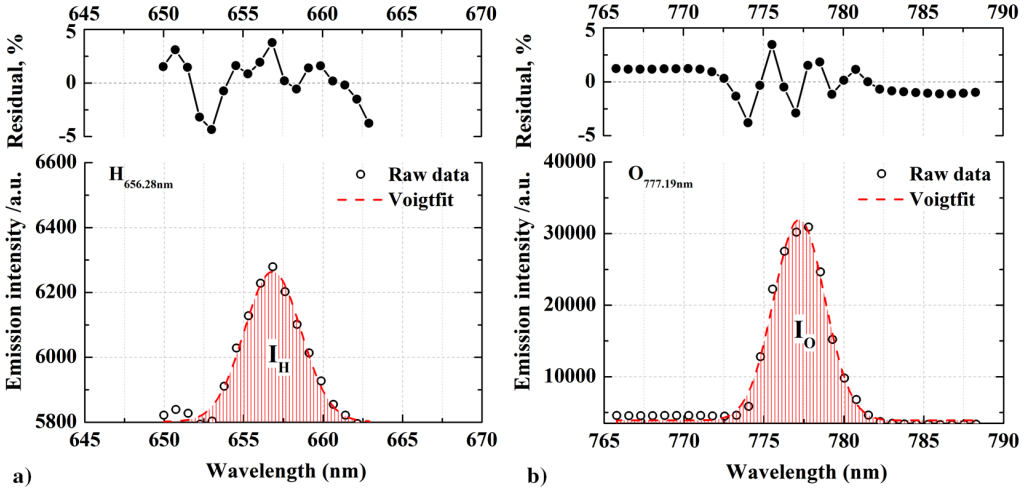

Fig. 8 Atomic emission intensity spectra (bottom plots) and residuals (top plots) from the measurements of flow rate of leaking water in test 2: a) emission spectrum of $H_{656.28}$, and b) emission spectrum of $O_{777.19}$.

are 0.0054 and 0.0040. The flow rate of the leaking water is derived from Eq. (9) and depends on temperature. With the magnetic field confinement of plasma electrons in the centermost region of the heater and the heat conduction between the high-temperature gas and the arc heater, there exists a radial thermal gradient in the flow field. As precise estimations of the temperature in the heater and the temperature gradients in the flow field are hard to achieve from experiments, we assume the temperature uncertainty to be within ± 1000 K so that the uncertainty in the flow rate may be calculated accordingly. Combined with the measurement uncertainty in the emission intensity ratio, Eq. (9), the detection limits for the mass flow of leaking water deduced for tests 1 and 2 are 1.85–0.99 g/s and 2.22–1.03 g/s, respectively, corresponding to equilibrium temperatures equal to 6000–8000 K and 5500–7500 K.

The above-detailed uncertainty analysis suggests that the experimental techniques need to be improved to increase the accuracy of temperature measurements. In future developments, the combination of the OES technique with multiple lines of sight to determine the radial distribution of the temperature is an important complement. In parallel, to reduce the uncertainties in the experimental spectral data, a statistical analysis of experimental data obtained from repeated runs under the same conditions will be performed. Other future work will involve the development of the engineering-level analysis method of leakage values based on the accumulation of more experimental data.

V. Conclusions

An optical emission spectroscopy (OES) system targeting $H_{656.28}$ and $O_{777.19}$ was developed to diagnose leakage failure of cooling water and to monitor concurrently the operating status in a 50-MW high-enthalpy arc-heated wind tunnel. A water-cooled disk coupled with an optical access port and an extension tube was designed to collect the radiation in the plenum region of the arc heater. Two tests with mass-average enthalpy settings of 18.7 and 16.4 MJ/kg were investigated. From the detailed analysis of the spectral characteristics of the normal and leakage spectra inside the arc heater, two different intensity determination methods for the $H_{656.28}$ and $O_{777.19}$ emissions were proposed and the intensity evolutions of $O_{777.19}$ and $H_{656.28}$ emission were determined. The initial beginning of micro-leakage for the two tests was determined, and the mass flow of the leaking water was deduced according to the integrated atomic line intensity ratio $I_{H_{656.28}}/I_{O_{777.19}}$ based on the local thermal equilibrium. An uncertainty analysis was performed to assess the measurement uncertainties from temperature determination and the integrated emission intensity. This work demonstrated the potential of using OES technique for leak detection of cooling water in a large-scale arc-heated facility.

Acknowledgments

This work was funded in part by the National Natural Science Foundation of China (No. 11802315) and the Pre-research Project of China Academy of Aerospace Aerodynamics. We thank Guoming Yang, Guosheng Lin, and Luping Zheng, who work at China Academy of Aerospace Aerodynamics, for providing help in arc heater operation. We thank Fei Yu, associate professor, from Shanghai Institute of Optics and Fine Mechanics, for his valuable comments to improve the paper.

References

[1] Takayanagi, H., Mizuno, M., Fujii, K., Suzuki, T., and Fujita, K., "Arc Heated Wind Tunnel Flow Diagnostics using Laser-Induced Fluorescence of Atomic Species," *47th AIAA Aerospace Sciences Meeting Including the New Horizons Forum and Aerospace Exposition*, AIAA Paper 2009-1449, 2009.

[2] Lin, X., Chen, L. Z., Zeng, H., Ou, D. B., and Dong, Y. H., "High Enthalpy Arc-Heated Plasma Flow Diagnostics by Tunable Diode Laser Absorption Spectroscopy," *Proceedings of SPIE 10173, Fourth International Symposium on Laser Interaction with Matter*, 2017, Paper 10173A. doi:10.1117/12.2266510

[3] Grinstead, J. H., Harris, C. L., Yeung, D., Scott, G. P., Porter, B. J., Graube, P., and Greenberg, R. B., "Next-Generation Laser-Induced Fluorescence Diagnostic Systems for NASA Arc Jet Facilities," *47th AIAA Aerospace Sciences Meeting Including the New Horizons Forum and Aerospace Exposition*, AIAA Paper 2009-1521, 2009.

[4] Birkan, M. A., "Arcjets and Arc Heaters—An Overview of Research Status and Needs," *Journal of Propulsion and Power*, Vol. 12, No. 6, 1996, pp. 1011–1017. doi:10.2514/3.24138

[5] Guy, R. W., Rogers, R. C., Puster, R. L., Rock, K. E., and Diskin, G. S., "The NASA Langley Scramjet Test Complex," *32nd Joint Propulsion Conference and Exhibit*, AIAA Paper 1996-3243, 1996.

[6] Kidd, F. G., Narayanaswamy, V., Danehy, P. M., Inman, J. A., Bathel, B. F., Cabell, K. F., Hass, N. E., Capriotti, D. P., and Drozda, T. G., "Characterization of the NASA Langley Arc Heated Scramjet Test Facility Using NO PLIF," *30th AIAA Aerodynamic Measurement Technology and Ground Testing Conference*, AIAA Paper 2014-2652, 2014.

[7] Stewart, D. A., Gökçen, T., and Chen, Y.-K., "Characterization of Hypersonic Flows in the AHF and IHF of NASA Ames Arc-Jet Facilities," *41st AIAA Thermophysics Conference*, AIAA Paper 2009-4237, 2009.

[8] Gülhan, A., Esser, B., and Koch, U., "Experimental Investigation of Reentry Vehicle Aerothermodynamic Problems in Arc-Heated Facilities," *Journal of Spacecraft and Rockets*, Vol. 38, No. 2, 2001, pp. 199–206. doi:10.2514/2.3670

[9] Smith, R., Wagner, D. A., and Cunningham, J., "A Survey of Current and Future Plasma Arc-Heated Test Facilities for Aerospace and

Commercial Applications," *36th AIAA Aerospace Sciences Meeting and Exhibit*, AIAA Paper 1998-146, 1998.
[10] Chau, S. W., Hsu, K. L., Lin, D. L., and Tzeng, C. C., "Experimental Study on Copper Cathode Erosion Rate and Rotational Velocity of Magnetically Driven Arcs in a Well-Type Cathode Non-Transferred Plasma Torch Operating in Air," *Journal of Physics D: Applied Physics*, Vol. 40, No. 7, 2007, pp. 1944–1952. doi:10.1088/0022-3727/40/7/017
[11] Sheeley, J. M., "Parametric Studies with an Arc Electrode Mass Loss Model," *10th AIAA/ASME Joint Thermophysics and Heat Transfer Conference*, AIAA Paper 2010-4658, 2010.
[12] Milos, F. S., and Shepard, C. E., "Thermal Analysis of an Arc Heater Electrode with a Rotating Arc Foot," *AIAA 28th Thermophysics Conference*, AIAA Paper 1993-2855, 1993.
[13] Mosley, K., Guile, A. E., and Dring, D., "Some Aspects of Electrode Erosion in Arc Heaters," *Journal of the Electrochemical Society*, Vol. 119, No. 10, 1972, pp. 1316–1320. doi:10.1149/1.2403985
[14] Durgapal, P., "Electrode Phenomena in High-Current, High-Pressure Arc Heaters," *Journal of Thermophysics and Heat Transfer*, Vol. 7, No. 3, 1993, pp. 412–417. doi:10.2514/3.434
[15] Painter, J. H., "High Pressure Arc Heater Electrode Heat Transfer Study," *AIAA Journal*, Vol. 13, No. 12, 1975, pp. 1555–1556. doi:10.2514/3.60581
[16] Durgapal, P., and Palmer, G., "Strongly Coupled Radiative Transfer and Joule Heating in an Arc Heater Electrode," *Journal of Thermophysics and Heat Transfer*, Vol. 8, No. 4, 1994, pp. 730–736. doi:10.2514/3.605
[17] Guile, A. E., Hitchcock, A. H., Dimoff, K., and Vijh, A. K., "Physical Implications of an Effective Activation Energy for Arc Erosion on Oxidised Cathodes," *Journal of Physics D: Applied Physics*, Vol. 15, No. 11, 1982, pp. 2341–2355. doi:10.1088/0022-3727/15/11/026
[18] Essiptchouk, A. M., Sharakhovsky, L. I., and Marotta, A., "The Effect of Surface Electrode Temperature on Cold Electrode Erosion Behaviour," *Plasma Sources Science and Technology*, Vol. 16, No. 1, 2007, pp. 1–6. doi:10.1088/0963-0252/16/1/001
[19] Teste, P., Leblanc, T., Andlauer, R., and Chabrerie, J.-P., "Copper Cathode Erosion by an Electric Arc—The Causes of the Variations of the Erosion Rate with the Electrode Gap," *Plasma Sources Science and Technology*, Vol. 10, No. 1, 2001, pp. 10–16. doi:10.1088/0963-0252/10/1/302
[20] Peters, J., Yin, F., Borges, C. F. M., Heberlein, J., and Hackett, C., "Erosion Mechanisms of Hafnium Cathodes at High Current," *Journal of Physics D: Applied Physics*, Vol. 38, No. 11, 2005, pp. 1781–1794. doi:10.1088/0022-3727/38/11/019
[21] Marotta, A., Sharakhovsky, L. I., and Essiptchouk, A. M., "The Best Arc Heater Regime for Minimum Copper Cathode Erosion," *11th International Congress on Plasma Physics*, Vol. 669, No. 1, 2003, pp. 22–25.
[22] Zhou, X., and Heberlein, J., "An Experimental Investigation of Factors Affecting Arc-Cathode Erosion," *Journal of Physics D: Applied Physics*, Vol. 31, No. 19, 1998, pp. 2577–2590. doi:10.1088/0022-3727/31/19/031
[23] Essiptchouk, A. M., Sharakhovsky, L. I., and Marotta, A., "Working Conditions of a Copper Cathode with Minimum Erosion," *Plasma Sources Science and Technology*, Vol. 12, No. 4, 2003, pp. 501–507. doi:10.1088/0963-0252/12/4/301
[24] Coulombe, S., and Meunier, J.-L., "Arc-Cold Cathode Interactions: Parametric Dependence on Local Pressure," *Plasma Sources Science and Technology*, Vol. 6, No. 4, 1997, pp. 508–517. doi:10.1088/0963-0252/6/4/008
[25] Marotta, A., and Sharakhovsky, L. I., "A Theoretical and Experimental Investigation of Copper Electrode Erosion in Electric Arc Heaters: I. The thermophysical Model," *Journal of Physics D: Applied Physics*, Vol. 29, No. 9, 1996, pp. 2395–2403. doi:10.1088/0022-3727/29/9/025
[26] Sharakhovsky, L. I., Marotta, A., and Borisyuk, V. N., "A Theoretical and Experimental Investigation of Copper Electrode Erosion in Electric Arc Heaters: II. The Experimental Determination of Arc Spot Parameters," *Journal of Physics D: Applied Physics*, Vol. 30, No. 14, 1997, pp. 2018–2025. doi:10.1088/0022-3727/30/14/009
[27] Sharakhovsky, L. I., Marotta, A., and Borisyuk, V. N., "A Theoretical and Experimental Investigation of Copper Electrode Erosion in Electric Arc Heaters: III. Experimental Validation and Prediction of Erosion," *Journal of Physics D: Applied Physics*, Vol. 30, No. 17, 1997, pp. 2421–2430. doi:10.1088/0022-3727/30/17/008
[28] Webb, B. T., and Sheeley, J. M., "Investigation of the Effects of Shear on Arc-Electrode Erosion Using a Modified Arc-Electrode Mass Loss Model," *55th AIAA Aerospace Sciences Meeting*, AIAA Paper 2017-0217, 2017.
[29] Lin, X., Chen, L. Z., Li, J. P., Li, F., and Yu, X. L., "Experimental and Numerical Study of Carbon-Dioxide Dissociation for Mars Atmospheric Entry," *Journal of Thermophysics and Heat Transfer*, Vol. 32, No.2, 2018, pp. 503–513. doi:10.2514/1.T5152
[30] Dikalyuk, A. S., Surzhikov, S. T., Kozlov, P. V., Shatalov, O. P., and Romanenko, Y. V., "Nonequilibrium Spectral Radiation Behind the Shock Waves in Martian and Earth Atmospheres," *44th AIAA Thermophysics Conference*, AIAA Paper 2013-2505, 2013.
[31] Boubert, P., and Rond, C., "Nonequilibrium Radiation in Shocked Martian Mixtures," *Journal of Thermophysics and Heat Transfer*, Vol. 24, No. 1, 2010, pp. 40–49. doi:10.2514/1.45385
[32] Babou, Y., Rivière, P., Perrin, M. Y., and Soufiani, A., "Spectroscopic Study of Microwave Plasmas of CO2 and CO2-N2 Mixtures at Atmospheroc Pressure," *Plasma Sources Science and Technology*, Vol. 17, No. 4, 2008, Paper 045010. doi:10.1088/0963-0252/17/4/045010
[33] Winter, M. W., and Prabhu, D. K., "Radiation Transport Analysis of Emission Spectroscopic Measurements in the Plenum Region of the NASA IHF Arc Jet Facility," *45th AIAA Plasmadynamics and Lasers Conference*, AIAA Paper 2014-2489, 2014.
[34] Meunier, J.-L., and Desaulniers-Soucy, N., "Erosion Rate Evaluation of Plasma Torch Electrodes from Measurements of the Emitted Metal Vapour Radiation," *Journal of Physics D: Applied Physics*, Vol. 27, No. 12, 1994, pp. 2522–2525. doi:10.1088/0022-3727/27/12/012
[35] Park, C., Raiche, G. A., Driver, D. M., Olejniczak, J., Terrazas-Salinas, I., Hightower, T. M., and Sakai, T., "Comparison of Enthalpy Determination Methods for an Arc-Jet Facility," *Journal of Thermophysics and Heat Transfer*, Vol. 20, No. 4, 2006, pp. 672–679. doi:10.2514/1.15744
[36] Jorgensen, L. H., and Baum, G. M., "Charts for Equilibrium Flow Properties of Air in Hypervelocity Nozzles," NASA TN D-1333, 1962.
[37] Winter, M. W., Raiche, G. A., Terrazas-Salinas, I., Hui, F. C. L., White, B., and Taunk, J. S., "Measurements of Radiation Heat Flux to a Probe Surface in the NASA Ames IHF Arc Jet Facility," *43rd AIAA Thermophysics Conference*, AIAA Paper 2012-3189, 2012.
[38] Winter, M. W., Prabhu, D. K., and Williams, W. W., "Determination of Temperature Profiles in the Plenum Region of the NASA IHF Arc Jet Facility from Emission Spectroscopic Measurements," *44th AIAA Thermophysics Conference*, AIAA Paper 2013-3016, 2013.
[39] Winter, M. W., Prabhu, D. K., Taunk, J. S., and Terrazas-Salinas, I., "Emission Spectroscopic Measurements in the Plenum of the NASA IHF Arc Jet Facility," *10th AIAA/ASME Joint Thermophysics and Heat Transfer Conference*, AIAA Paper 2010-4522, 2010.
[40] Laux, C. O., "Optical Dignostics and Radiative Emission of Air Plasmas," Ph.D. Thesis, Stanford Univ., Stanford, CA, 1993.